Analysis of D/T Fuel Ratio in Power Plant Plasmas Using Integrated Equilibrium-Transport Simulation Code TOTAL

Tetsutarou OISHI, Kozo YAMAZAKI, Hideki ARIMOTO and Tatsuo SHOJI

Nagoya University, Chikusa-ku, Nagoya 464-8603 Japan

Pellet injection to D-T burning plasmas was analyzed using an integrated equilibrium-transport simulation code, TOTAL, for both tokamak and helical reactors. The condition of pellet injection required for the formation of an internal transport barrier and the dependence of plasma parameters in the steady self-burning state on the D/T ratio in the pellet were investigated. A simulation with different D/T ratios in the pellet revealed that the operational region of temperature and density varies with the D/T ratio. When a deuterium-rich pellet was employed, the amount of tritium to be used in the reactor was approximately 30%-40% less than that when the D/T ratio was 1.

1. Inroduction

The deuterium/tritium (D/T) fuel ratio is a key parameter for determining the output power of nuclear fusion energy reactors. Several fueling methods, such as pellet injection, compact torus injection, neutral beam injection, and gas puffing, have been proposed for fusion reactors to control the D/T fuel ratio.

To numerically analyze the relationship among the fueling methods, D/T fuel ratio, and output reactor power, we have applied the toroidal transport analysis linkage (TOTAL) simulation code to model the fuel supply in D-T burning plasmas in both tokamak and helical reactors [1]. The two-dimensional or three-dimensional equilibrium calculation using the APOLLO [2] or VMEC [3] code and one-dimensional transport simulation model are combined in the TOTAL code. In this study, we focus on pellet injection as a fueling method. The neutral gas shielding model with a mass relocation model is included in the code to calculate the profile of pellet penetration.

This paper investigates the conditions of pellet injection required for improved confinement, represented by formation of the internal transport barrier (ITB) and the dependence of plasma parameters in the steady self-burning state on the D/T ratio in the pellet.

2. Simulation Methods
2.1 Transport model

We have employed a transport model considering the suppression of turbulence by $E \times B$ shear and the resulting improvement of confinement [4]. This model focuses on the ion temperature gradient (ITG) mode [5] as the representative turbulence. The thermal diffusion coefficient χ is

author's e-mail: t-oishi@mail.nucl.nagoya-u.ac.jp

determined by

$$\chi = \chi_{NC} + \chi_{AN} \times F(\omega_{E \times B}/\gamma_{ITG}), \qquad (1)$$

where χ_{NC} and χ_{AN} are the neoclassical and anomalous thermal diffusion coefficients, respectively. In the present study, the Bohm and gyro-Bohm mixed model [6] is employed to express χ_{AN},

$$\chi_{AN} = 4.0\chi_{Bohm} + 0.5\chi_{Gyro-Bohm}, \qquad (2)$$

$$\chi_{Bohm} = 4 \times 10^{-5} R \left| \frac{\nabla(n_e T_e)}{n_e B_\phi} \right| q^2, \qquad (3)$$

$$\chi_{Gyro-Bohm} = 5 \times 10^{-6} \sqrt{T_e} \left| \frac{\nabla T_e}{B_\phi^2} \right|. \qquad (4)$$

$F(\omega_{E \times B}/\gamma_{ITG})$ in Eq. (1) is the improvement factor [7], defined as

$$F(\omega_{E \times B}/\gamma_{ITG}) = \frac{1}{1 + (\tau\,\omega_{E \times B}/\gamma_{ITG})^\gamma}. \qquad (5)$$

$\omega_{E \times B}$ is the $E \times B$ flow shearing rate [8], defined as

$$\omega_{E \times B} = \left| \frac{RB_\theta}{B_\phi} \frac{\partial}{\partial r}\left(\frac{E_r}{RB_\theta}\right) \right|, \qquad (6)$$

and γ_{ITG} is the linear growth rate of the ITG mode, defined as

$$\gamma_{ITG} = \frac{(\eta_i - 2/3)^{1/2}\,|s|\,c_i}{qR}, \quad s = \frac{r}{q}\left(\frac{dq}{dr}\right), \qquad (7)$$

where $\eta_i = L_n/L_T$ is the ratio between the ion density scale length L_n and the ion temperature scale length L_T, s is the magnetic shear, and $c_i = (T_i/m_i)^{1/2}$ [5]. Each proportional coefficient for χ_{Bohm} and $\chi_{Gyro-Bohm}$ in Eq. (2) and parameters τ and γ in Eq. (5) ($\tau = 2.0$ and $\gamma = 4.0$ for tokamaks,

and $\tau = 15.0$ and $\gamma = 2.0$ for helicals) were determined by comparison with experimental data from the reversed shear discharge with an ITB in the JT-60U tokamak (#29728, #32423) [9] and ITB discharge in the large helical device (LHD) (#26943) [10]. In the tokamak reactor, the profile of safety factor q with reversed shear is given as an input parameter at the start of the calculation. A polynomial function having a minimum value at around $\rho = 0.65$ was used to describe the q profile of reversed shear. Typical values of q in this profile are 2.5 ($\rho = 0$), 2.0 ($\rho = 0.65$), and 4.4 ($\rho = 1.0$). Profiles of the poloidal magnetic fields and plasma current are calculated to satisfy the q profile and total plasma current at each time step. The factor $[(T_e (\rho = 0.8)$-$T_e (\rho = 1.0))/T_e (\rho = 1.0)]$ is multiplied by χ_{Bohm} to express the edge effect of H-mode behavior in this calculation. By using Eqs. (1) and (5), we assume that the anomalous transport is suppressed when $\omega_{E \times B}$ exceeds γ_{ITG}.

The anomalous part of the particle diffusion coefficient D_{AN} is calculated as

$$D_{AN} = (0.3 + 0.7\rho) \frac{\chi_{eAN}\chi_{iAN}}{\chi_{eAN} + \chi_{iAN}}. \qquad (8)$$

2.2 Pellet injection model

The neutral gas shielding (NGS) model [11] gives the ablation rate along the pellet path l as

$$\frac{dN}{dl} = 4.38 \times 10^3 N^{0.444} n_e^{0.333} T_e^{1.64} M_i^{-0.333}/V_p, \qquad (9)$$

where N is the number of atoms in the pellet, M_i is the pellet mass, and V_p is the pellet injection velocity.

It is widely recognized that pellet injection from the high-field-side (HFS) is effective for injecting pellets deep into the core region of a tokamak plasma [12]. To simulate HFS pellet injection in tokamaks, we apply the mass relocation model [13], which describes the drift of the plasmoid generated by pellet ablation. The mass relocation model gives the displacement δx ($x = r/a$, normalized minor radius) of the plasmoid in the major-radius direction as

$$\delta x = \delta r/a \sim \delta\psi/\Delta\psi, \qquad (10)$$

where ψ, $\delta\psi$, and $\Delta\psi$ are the poloidal flux, polodal flux perturbation, and total poloidal flux, respectively. $\delta\psi$ is obtained by the scaling

$$\delta\psi = q\beta B_\phi (1 + qL_c/a)^{-1} a^{-1} \delta n r_0^2 (n + \langle\delta n\rangle)^{-1}, \qquad (11)$$

and $\Delta\psi$ is

$$\Delta\psi = \psi(a) - \psi(0) \sim \int r dr/q, \qquad (12)$$

where r_0 and L_c are the radius and height of the cylindrical plasmoid, respectively.

3. Simulation Results

The plasma parameters of an ITER-like tokamak reactor with reversed shear configuration and an LHD-like

Table 1 Plasma parameters of the tokamak and helical reactors.

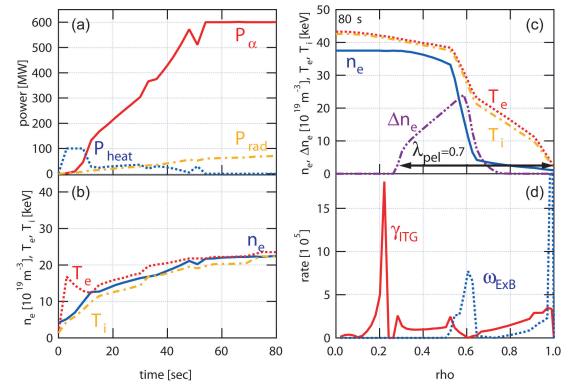|	Tokamak	Helical
major radius R_p [m]	5.29	16.8
minor radius a_p [m]	1.25	2.8
toroidal field B_{z0} [T]	7.11	4.21
plasma current I_p [MA]	13.0	-
α heating power [MW]	600.0	470.0
ellipticity	2.0	-
triangularity	0.5	-

Fig. 1 Simulation results for the reversed shear tokamak reactor with pellet-injection fueling. The normalized penetration length $\lambda_{pel} = 0.7$. Left: temporal evolution of (a) alpha heating power P_α, auxiliary heating power P_{heat}, and radiation power loss P_{rad}, and (b) averaged electron density $<n_e>$, electron temperature $<T_e>$, and ion temperature $<T_i>$. Right: radial profiles of (c) electron density n_e, electron temperature T_e, ion temperature T_i, and pellet deposition Δn_e, and (d) growth rate of the ion temperature gradient mode γ_{ITG}, and the $E \times B$ shearing rate $\omega_{E\times B}$.

helical reactor with the $l/m = 2/10$ heliotron configuration as simulation targets are determined using the reactor design system Physics-Engineering-Cost (PEC) code [14]. The main plasma parameters are shown in Table 1. These parameters refer to 1 GW of electrical power generated by the D-T reaction. In this simulation, the pellet injection frequency and auxiliary heating power are feedback-controlled such that the density and temperature increase in the initial state, and then the alpha particle heating power maintains a value of 600 MW for a tokamak reactor and 470 MW for a helical reactor during the steady state.

3.1 Conditions of pellet injection required to form an ITB

Figure 1 shows the simulation results for the reversed shear tokamak reactor with pellet-injection fueling. On the left is the temporal evolution of (a) alpha heating power P_α, auxiliary heating power P_{heat}, and radiation power loss P_{rad}, and (b) averaged electron density $<n_e>$, electron temperature $<T_e>$, and ion temperature $<T_i>$. Figure 1 (c) shows the radial profile of electron density n_e, electron
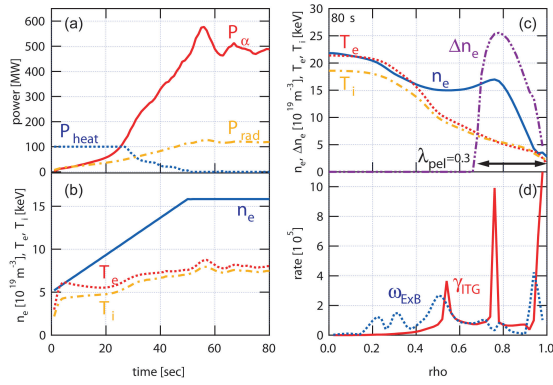
Fig. 2 Simulation results for the helical reactor with pellet injection fueling with $\lambda_{pel} = 0.3$. Left: temporal evolution of (a) P_α, P_{heat}, and P_{rad}, and (b) $<n_e>$, $<T_e>$, and $<T_i>$. Right: radial profiles of (c) n_e, T_e, T_i, and Δn_e, and (d) γ_{ITG} and $\omega_{E\times B}$.

temperature T_e, ion temperature T_i, and pellet deposition Δn_e. The temperature profile has a steep gradient at $\rho = 0.5\sim0.65$. The maximum value of the normalized temperature gradient $R/L_{Te} \equiv R/(T_e/\nabla T_e)$ is about 20 at $\rho = 0.65$. The pellet ablation profile shows that the pellet penetrated up to $\rho = 0.3$. We include the value λ_{pel} as an indicator of the penetration depth measured from the plasma edge, which is normalized by the plasma minor radius. $\lambda_{pel} = 1$ indicates that the pellet has reached the plasma center. The case shown in Fig. 1 corresponds to $\lambda_{pel} = 0.7$. Figure 1 (d) shows the growth rate of the ion temperature gradient mode γ_{ITG} and the $E \times B$ shearing rate $\omega_{E\times B}$. $\omega_{E\times B}$ exceeds γ_{ITG} at $\rho = 0.55\sim0.7$, which corresponds to the region of ITB formation.

On the other hand, no ITB forms if the pellet penetration depth is shallow. A simulation with a varied λ_{pel} revealed that an ITB forms when $\lambda_{pel} > 0.35$ [15]. This corresponds to pellet injection deeper than $\rho = 0.65$, where the magnetic shear is almost zero and γ_{ITG} is small. Therefore, if a large electric field shear exists at $\rho = 0.65$, $\omega_{E\times B}$ becomes much larger than γ_{ITG}, improving the confinement. This condition can be satisfied by deep pellet penetration and by increasing the density at regions interior to $\rho = 0.65$, which determines the threshold pellet penetration depth to form an ITB.

Figure 2 shows the simulation results for the helical reactor with a normalized penetration length $\lambda_{pel} = 0.3$. A steep temperature gradient was observed at $\rho = 0.2\sim0.5$. The maximum value of R/L_{Te} is about 20 at $\rho = 0.5$, which is comparable to that of tokamaks. However, unlike the case in tokamaks, ITB formation is independent of pellet penetration depth. In the helical reactor, the radial profile of the electric fields is determined by the ambipolar flux of ions and electrons. In the conditions employed in this study, the shear of the ambipolar electric field is located at around $\rho = 0.2\sim0.5$. Therefore, $\omega_{E\times B}$ becomes larger than γ_{ITG} in this region as shown in Fig. 2 (d), improving the confinement.
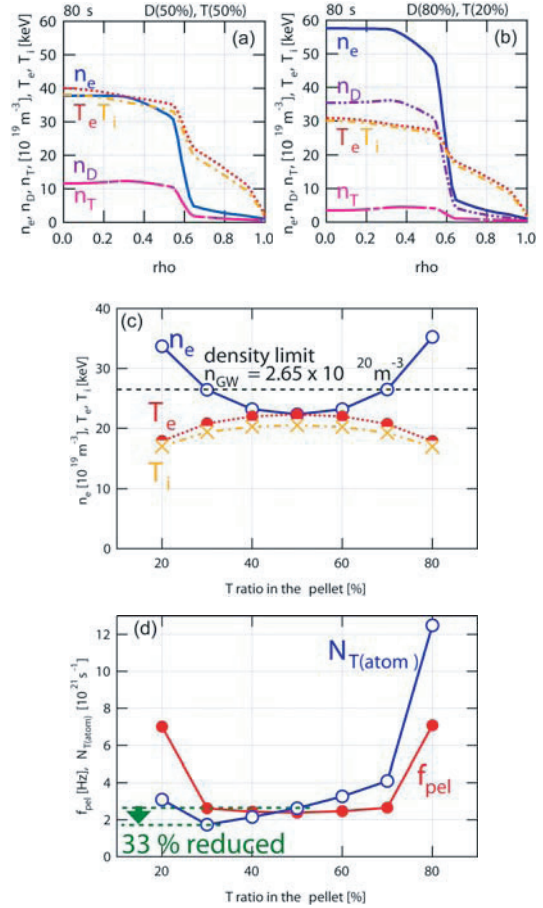

Fig. 3 Simulation results the reversed shear tokamak reactor in the steady self-burning state with varying D/T ratio in the pellet. Radial profiles of n_D, n_T, n_e, T_e, and T_i with D/T ratios of 50/50 (a) and 80/20 (b). (c) $<n_e>$, $<T_e>$, and $<T_i>$ versus tritium ratio in the pellet. (d) Pellet injection frequency f_{pel} and tritium consumption per unit time $N_{T(atom)}$ versus tritium ratio in the pellet.

The density profile in the helical reactor has a peaked profile compared to that in the tokamak reactor. This arises from the difference in the particle diffusion coefficient profile between tokamak and helical reactors. The anomalous part of the particle diffusion coefficient D_{AN} is calculated in Eq. (8) by using anomalous thermal diffusion coefficients. In the helical reactor simulated here, the anomalous thermal diffusion coefficients were suppressed at around $\rho = 0.2\sim0.5$ because $\omega_{E\times B}$ exceeded γ_{ITG} in this region as shown in Fig. 2 (d). This suppresses D_{AN} and forms a particle transport barrier at around $\rho = 0.2\sim0.5$. This barrier has a greater radial width and a lower gradient than those of a tokamak. This shape of the barrier makes the density profile peaked in the helical reactor.

3.2 Effect of D/T ratio in the pellet

In the previous section, we modeled pellets consisting of 50% deuterium and 50% tritium. Now we perform a simulation while varying the density ratio of D/T in the pellet. In this calculation, the alpha heating powers were
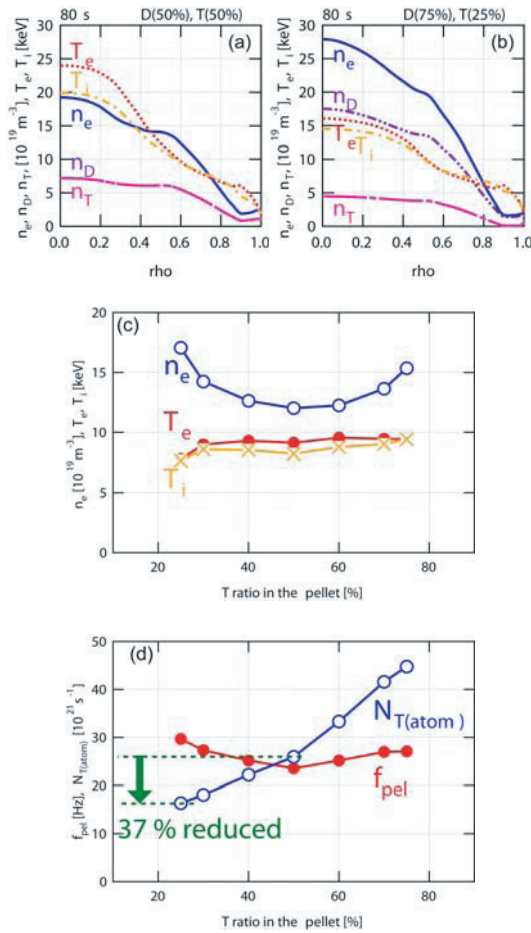
Fig. 4 Simulation results for the helical reactor in the steady self-burning state with varying D/T ratio in the pellet. Radial profiles of n_D, n_T, n_e, T_e, and T_i with D/T ratios of 50/50 (a) and 80/20 (b). (c) $\langle n_e \rangle$, $\langle T_e \rangle$, and $\langle T_i \rangle$ versus tritium ratio in the pellet. (d) f_{pel} and $N_{T(atom)}$ versus tritium ratio in the pellet.

fixed at the values in Table 1 even if the D/T ratio in the pellet varied.

Figure 3 shows the simulation results for the reversed shear tokamak reactor in the steady self-burning state with a varying D/T ratio in the pellet. λ_{pel} is controlled to satisfy the conditions for forming an ITB. The radial profiles of n_D, n_T, n_e, T_e, and T_i with D/T ratios of 50/50 and 80/20 are shown in Figs. 3 (a) and (b), respectively. The density profiles of deuterium and tritium are identical in Fig. 3 (a), but they are quite different in Fig. 3 (b). In this case, the short supply of tritium is compensated for by increasing the amount of deuterium. Figure 3 (c) shows $\langle n_e \rangle$, $\langle T_e \rangle$, and $\langle T_i \rangle$ plotted against the tritium ratio in the pellet. As the D/T ratio becomes asymmetrical, a higher density is required and the temperature decreases. With an asymmetrical D/T ratio, the pellet injection frequency f_{pel} which is defined by the number of pellets injected to the reactor per unit time, increases. Thus, we can evaluate the tritium consumption per unit time, $N_{T(atom)}$, by multiplying the pellet frequency and the tritium ratio in the pellet for each tritium

ratio. Figure 3 (d) shows the pellet frequency and tritium consumption per unit time as a function of tritium ratio in the pellet. The minimum value of $N_{T(atom)}$ is 33% smaller than that with a D/T ratio of 50/50.

Figure 4 shows the results of the same analysis described above for the helical reactor. Similar behavior to that in tokamaks was confirmed; higher density and high pellet injection frequency are required as the D/T ratio becomes asymmetrical. Figure 4 (d) shows that the minimum value of $N_{T(atom)}$ is 37% smaller than that with a D/T ratio of 50/50. These results suggest that the amount of tritium used in the reactor can be reduced by applying an appropriate D/T ratio in the pellet and an appropriate operational region of density and temperature.

4. Summary

Pellet injection to D-T burning plasmas was analyzed using the integrated equilibrium-transport simulation code TOTAL. In a tokamak reactor, pellet penetration deeper than the location where the magnetic shear $dq/dr = 0$ was confirmed to be effective in suppressing anomalous transport and forming an ITB. In a helical reactor, ITB formation was independent of the depth of pellet penetration. A simulation with different D/T ratios in the pellet revealed that the operational region of temperature and density varies with the D/T ratio. When a deuterium-rich pellet was employed, the amount of tritium to be used in the reactor was approximately 30%-40% less than that when the D/T ratio was 1.

Based on these results, a proposal of tritium reduction scenario for fusion reactor operation, including the start-up phase of the reactor, is planned for the future. A method of controlling fusion power by controlling the D/T fuel ratio can be also considered.

[1] K. Yamazaki and T. Amano, Nucl. Fusion **32**, 633 (1992).
[2] K. Yamazaki *et al.*, Nucl. Fusion **25**, 1543 (1985).
[3] S. P. Hirshman *et al.*, Comput. Phys. Commun. **43**, 143 (1986).
[4] Y. B. Kim *et al.*, Phys. Fluids B **3**, 384 (1991).
[5] A. L. Rogister, Nucl. Fusion **41**, 1101 (2001).
[6] M. Erba *et al.*, Plasma Phys. Control. Fusion **39**, 261 (1997).
[7] Y. Higashiyama *et al.*, Plasma Fusion Res. **3**, S1048 (2008).
[8] T. S. Harm and K. H. Burrell, Phys. Plasmas **2**, 1648 (1995).
[9] T. Fujita *et al.*, Phys. Rev. Lett. **78**, 2377 (1997).
[10] T. Shimozuma *et al.*, Plasma Phys. Control. Fusion **45**, 1183 (2003).
[11] L. R. Bayler *et al.*, Fusion Technol. **34**, 425 (1998).
[12] A. R. Polevoi and M. Shimada, Plasma Phys. Control. Fusion **43**, 1525 (2001).
[13] P. Parks *et al.*, Nucl. Fusion **17**, 539 (1977).
[14] K. Yamazaki *et al.*, Fusion Eng. Des. **81**, 2743 (2006).
[15] T. Oishi *et al.*, J. Plasma Fusion Res. SERIES **8**, 1004 (2009).